ON SUSPENDED BARITE AND TIlE OXYGEN MINIMUM IN THE SOUTHERN OCEAN

Frank Dehairs, L. Goeyens, N. Stroobants, P. Bernard, Catherine Goyet, Alain Poisson, R. Chesselet

GLOBAL BIOGEOCHEMICAL CYCLES, VOL. 4, NO. 1, PAGES 85-102, MARCH 1990

ON SUSPENDED BARITE AND THE OXYGEN MINIMUM IN THE SOUTHERN OCEAN

F. Dehairs,[1] L. Goeyens,[1] N. Stroobants,[1]
P. Bernard,[2] C. Goyet,[3] A. Poisson,[3] and
R. Chesselet[4]

Abstract. Particulate Ba profiles were measured in the Indian sector of the southern ocean. The largest fraction (>80%) of this barium is present as barite microcrystals. The profiles of total barium are characterized by a subsurface maximum between 200 and 500 m depth in the vicinity of the oxygen minimum. Highest barium values are found just south of the Polar Front, while lowest values occur close to the Antarctic Divergence. Between the divergence and the Polar Front a tight inverse relationship is observed between oxygen in the oxygen minimum and barium in the barium maximum. This relationship disappears north of the Polar Front. Since suspended barite is known to be of biological origin, the correlation of barite with oxygen suggests that the observed decrease of oxygen in the oxygen minimum, between the divergence and the Polar Front is due to local consumption of oxygen. It is proposed that deep low oxygen water is advected towards the Divergence where upwelling occurs and where this water subsequently partly spreads out to the north, north-east, as entrained by the Antarctic Circumpolar Current. Oxidation of locally produced organic matter, with which barite crystals are associated, consumes oxygen and sets free individual discrete barites. As a result, oxygen decreases and barite increases away from the divergence, with barite integrating former biological processes.

[1]Analytische Chemie (ANCH), Vrije Universiteit Brussel, Brussels, Belgium.
[2]Departement Scheikunde, Universitaire Instelling Antwerpen, Wilrijk, Belgium.
[3]Laboratoire de Physique et Chimie Marine (LPCM), Université Pierre et Marie Curie, Paris, France.
[4]Institut National des Sciences de l'Univers (INSU), Centre National de la Recherche Scientifique, Paris, France.

Paper number 90GB01599.
0886-6236/90/90GB-01599$10.00

INTRODUCTION

The important role of biological activity in the barium cycle was understood in earlier sedimentological studies, from the observed coincidence between high barite content in the sediments and presence of high plankton productivities in the overlying surface waters [Goldberg and Arrhenius, 1958; Arrhenius and Bonatti, 1965; Church, 1970, 1976; Hanor, 1972].

The importance of biological control was confirmed from data on suspended matter collected during the Geochemical Ocean Sections (GEOSECS) program (1972-1979) showing barium in suspended matter to occur mainly as barite microcrystals and barite content to be positively correlated with plankton activity [Dehairs et al., 1980]. This is confirmed by Bishop [1989], who states that Ba appears to be a good indicator of ocean regions with intense organic production. Furthermore, data for sediment traps [Dymond, 1986] and deep-sea sediments [Schmitz, 1987] indicate the particulate barium-barite flux to be a proxy of the organic carbon flux. These latter studies show that despite the undersaturation of the water column for $BaSO_4$ [Church, 1970, 1976; Church and Wolgemuth, 1972], barite behaves semiconservatively with respect to organic matter. However, its slow dissolution rate in the undersaturated water column was estimated to be sufficient to account for the main part of the dissolved barium input to the deep ocean [Dehairs et al., 1980; Rhein and Schlitzer, 1989].

While the general picture of biological control is now well established, details of the mechanisms of this

control are lacking. Active intracellular production of barite is known to occur for some marine and freshwater algal and protozoan species [Hubert et al.,1975; Gayral and Fresnel, 1979; Brook et al., 1980; Finlay et al., 1983]. Chow and Goldberg [1960] proposed that formation of barite could also take place in supersaturated microenvironments composed of biogenic detritus. Evidence for barite association with microenvironments was indeed found during GEOSECS [Dehairs, 1979]. Furthermore, the use of high volume in-situ filtration devices clearly showed, for surface waters of the NW and SE Atlantic Ocean, the presence of barite in large aggregates of biogenic detritus enriched with diatom tests [Bishop, 1988]. Bishop also shows that below the surface waters barite is seen to shift from a large size fraction (> 53 μm) to a smaller size fraction (< 53 μm), probably as a result of aggregate breakdown. This process explains the subsurface particulate Ba maximum generally observed for profiles obtained using small volume, Niskin-type, samplers [Dehairs et al., 1980].

The aim of our research is to investigate further on the process of barite formation in the water column and on the usefulness of barite as a tracer of productivity. We specifically investigate on the mode of barite production (passive and/or active) as well as on the extent the subsurface Ba maximum, decribed above, reflects organic matter breakdown and oxidation. In the present study we compare the particulate Ba and dissolved oxygen data set we obtained for the Indien Géophysique Océan 3 (INDIGO 3) cruise in the southern ocean (Indian Ocean sector; January-February, 1987; R/V *Marion Dufresne*), during which marked oxygen minima and barium maxima were observed in subsurface waters. During INDIGO 3 we also investigated the possible impact of heterotrophic activity on barite formation by comparing rates of organic matter mineralization with occurrence of barite in suspended matter. Prior to this study, only a small data set on particulate barium, obtained during the GEOSECS Atlantic program, existed for the southern ocean [Dehairs, 1979].

EXPERIMENT

The Sampling and Experiments at Sea

The area investigated is shown in Figure 1. The positions of the main frontal systems are indicated, as deduced from the surface water temperature profile [Goffart and Hecq, 1988]. Their latitudinal positions are close to those given by Lutjeharms et al. [1983] for the same general area.

Suspended matter samples were taken using 30-L Niskin bottles mounted on a hydrowire. Casts generally went down to 2000 m, but for some stations the whole water column was sampled. The Niskin bottles used were slightly modified to locate the outlet in the lower lid so as to ensure collecting rapidly settling large particles on the filter membranes during filtration. Suspended matter was collected on cellulose-ester membranes (MF-Millipore AAWP: ø, 47 mm; porosity, 0.8 μm), by applying pressure (0.3 bar) of filtered air at the top outlet of the bottles. In this way, approximately 3.5 hours were necessary to filter a 30-L sample. After filtration the filters were rinsed with 20 mL deionized water adjusted to pH 7, for carbonate particle preservation, and dried at 50°C. Samples were stored in polycarbonate petri dishes at ambient temperature. Several blank filters were treated similarly. Samples were analyzed a few months later in the shore-based laboratory in Brussels.

It is important to stress here the fact that the type of sampler used allows for a representative sampling of the small and slowly settling particles, constituting the bulk of the suspended matter mass. Fast settling large particles, such as fecal pellets and aggregates, are not sampled in a statistically significant way by this sampling technique, as indicated by Bishop and Edmond [1976]. Such particles represent only a small fraction of the total suspended matter mass but carry most of the vertical flux. However, within the euphotic layer the large particle fraction can represent up to 50% of the total particle mass [Bishop and Edmond, 1976]. Their quantitative sampling requires the use of high-volume (several cubic meters) sampling and filtration devices as used by Bishop [1988].

Remineralization rates were determined using isotope dilution experiments. One liter water samples were spiked with labelled (^{15}N) ammonium and incubated in glass bottles at the temperature of surface seawater for 24 hours or more [Goeyens and Dehairs, 1989]. The mass balance equations for $N\text{-}NH_4$ and for ^{15}N, used to estimate regeneration as well as incorporation of ammonium, are those described by Harrison [1983].

Measurements on Board the Ship

Salinity was measured on the practical salinity scale using a Guildline salinometer. Dissolved oxygen was measured by Winkler titration. Nitrate and ammonium were analyzed with a Technicon autoanalyzer AA II using the method described by Armstrong et al. [1967] and Grasshoff [1969].

Measurements in the Shore-Based Laboratory in Brussels

For complete dissolution of the barite an alkaline fusion technique derived from the one described by Burman et al. [1978] is used. Before the fusion process is performed, the organic filter substrate is oxidized by adding concentrated HNO_3 and H_2O_2 (1 and 3 mL respectively; all Merck Suprapur) to the filters in platinum crucibles and by heating until complete dessication. The fusion itself is carried out with a $LiBO_2$ flux (50 mg per filter; Johnson & Matthey, Specpure) at 1100°C for 1 hour. The formed glassy pearl is then dissolved in HNO_3 under heating. The solution is brought to 10 mL with deionized water and is 5% in $LiBO_2$ and 4% in HNO_3. The determination of barium is carried out by inductively coupled plasma - optical emission spectrometry (ICP-OES), using a Jobin-Yvon 48 simultaneous spectrometer. The spectrometer is equiped with a demountable torch (Durr / Jobin-Yvon). The sample is introduced using a concentric pneumatic glass nebulizer (Meinhard type C). The nebulizer argon flow is previously wetted with deionized water, to avoid clogging by salt crystalisation in the nebulizer tip.

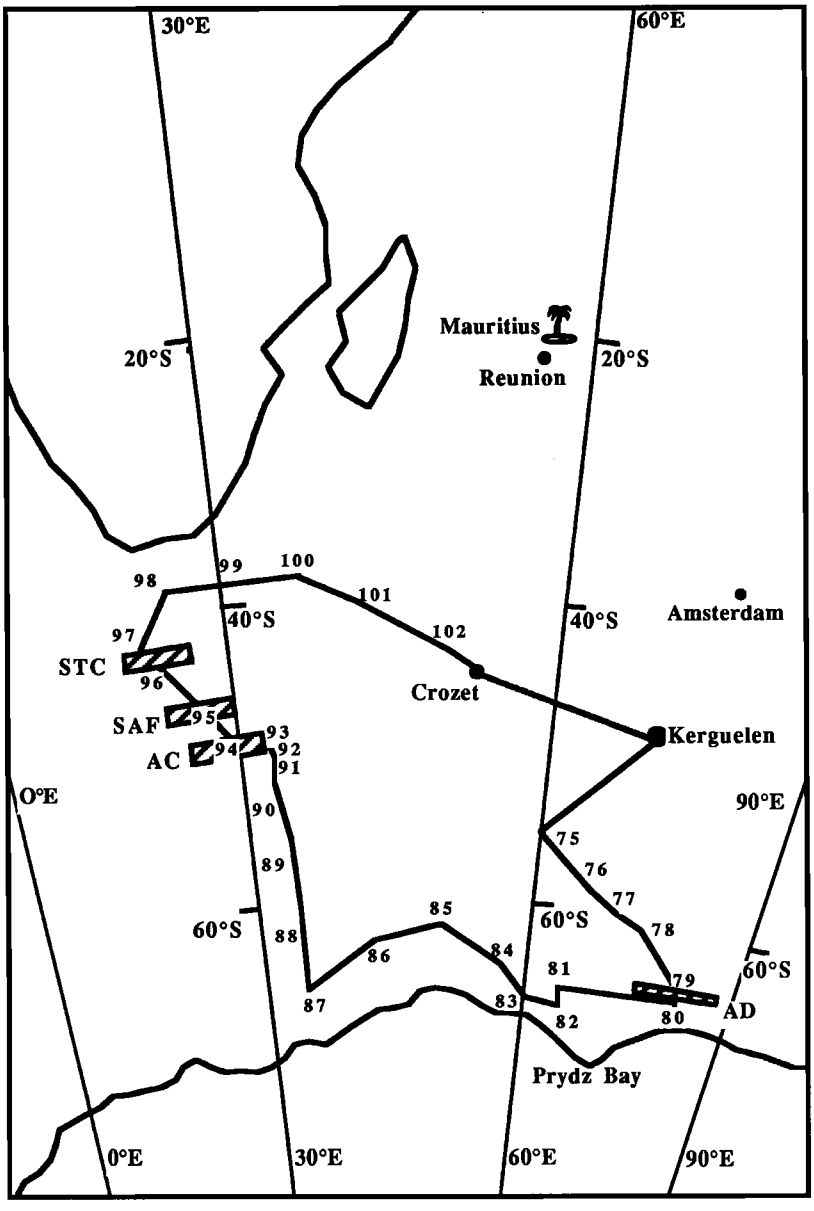

Fig. 1. INDIGO 3 cruise track in the Indian sector of the southern ocean. STC, Subtropical Convergence; SAF, Subantarctic Front; AC, Antarctic Convergence, or Polar Front; AD, Antarctic Divergence.

Operating power is generally 1.8 kW. The argon flows are as follows: coolant, 19 L min^{-1}; sample, 0.58 L min^{-1}; auxiliary flow, 0.15 L min^{-1}.

Barium standards (Titrisol, Merck) are prepared in the same matrix as the samples. Precision of the ICP determination (five consecutive measurements on the same solution) is between 1 and 5% for final solutions containing between 10 and 50 μg L^{-1} barium and better than 1.5% for solutions exceeding 50 μg L^{-1}. Recovery of barium was checked using blank filter membranes spiked with 2 μg barium. This showed a recovery of 100%. Procedural blanks were observed to contain 33 ± 15 ng Ba per filter (n=5).

Abundances of ^{15}N are determined by emission spectrometric analysis with a Jasco, Model NIA-1, ^{15}N analyzer. Ammonium is separated from its seawater matrix by addition of excess hydroxide and trapped in acid before conversion into molecular nitrogen by the modified Dumas method [L.Goeyens et al., manuscript in preparation, 1990]. The measurement of the ^{15}N abundances is calibrated with certified standards (Hikari, Kogyo Co., Ltd).

RESULTS

The total data set for suspended matter profiles of INDIGO 3 is given elsewhere [Dehairs and Goeyens, 1989; Poisson et al., 1990]. The barium data for 10 typical stations are shown in Table 1 together with data for potential temperature, salinity, σ_θ, dissolved oxygen, calculated pCO_2 (from measured total alkalinity and total inorganic carbon), and chlorophyll-*a* (Chl-*a* data, from Goffart and Hecq [1988]).

For one station (76) we checked if the total barium measured by ICP was indeed carried mainly by barite, as observed earlier [Dehairs et al., 1980]. To that purpose, known additional fractions (about 10 L) of the seawater volume sampled at 500 and 700 m (i.e., oxygen minimum and below oxygen minimum) were filtered on Nuclepore membranes (0.4 µm pore size; ø 47 mm) for scanning electron microscope - electron microprobe (SEM-EMP) investigations. These were carried out with a JEOL JXA 733 Superprobe and Tracor Northern

TABLE 1. Profiles of Salinity, Potential Temperature, Density, Dissolved Oxygen, Particulate Barium and Partial Pressure of CO_2 for Stations 75, 76, 78, 81, 86, 87, 88, 89, 90, 95, 98, and 99

Depth, m	Salinity, ppt	Tpot, °C	σ_θ	O_2, µmol kg^{-1}	Ba, pmol kg^{-1}	pCO_2, µatm
Station 75: 56°29' S, 63°09' E; Water Column, 4777 m						
-10	33.922	2.326	27.084	330	110	325
-20	33.922	2.316	27.084	330	177	340
-35	33.922	2.319	27.084	330	174	351
-50	33.924	2.311	27.086	331	191	347
-75	33.934	1.678	27.143	334	81	345
-100	33.958	0.945	27.212	336	84	345
-200	34.105	0.860	27.335	289	398	413
-300	34.436	1.910	27.528	190	656	557
-400	34.540	2.020	27.603	176	654	577
-500	34.604	2.066	27.651	175	401	563
-600	34.653	2.078	27.689	177	340	548
-700	34.681	2.051	27.714	180	329	524
-800	34.702	1.976	27.736	183	237	525
-900	34.714	1.901	27.752	186	303	512
-1000	34.726	1.832	27.767	189	322	525
-1100	34.738	1.777	27.781	193	259	520
-1300	34.749	1.633	27.800	198	174	490
-1500	34.750	1.524	27.817	202	198	-
Station 76: 59°28' S, 69°55' E; Water Column, 4410						
-10	33.665	1.344	26.956	342	151	318
-41	33.67	1.225	26.963	343	408	330
-72	34.691	-0.267	27.075	349	145	-
-92	33.793	-1.226	27.154	350	66	323
-123	33.87	-1.401	27.244	343	48	330
-153	33.974	-0.712	27.289	315	112	-
-179	34.119	-0.076	27.35	288	201	-
-204	34.254	0.587	27.413	261	271	448
-256	34.39	1.57	27.512	207	408	546
-307	34.454	1.788	27.564	187	407	571
-382	34.561	1.926	27.707	177	541	591
-478	34.618	1.988	27.662	175	341	
-573	34.654	2.003	27.701	177	395	566
-669	34.682	1.993	27.721	181	237	541
-764	34.704	1.964	27.746	185	290	525
-860	34.724	1.916	27.76	189	247	-
-955	34.735	1.858	27.772	193	219	507
-1098	34.742	1.743	27.788	197	175	481
-1242	34.748	1.603	27.801	202	169	461
-1433	34.737	1.425	27.812	203	305	469
-1591	34.745	1.223	27.82	204	133	-
-1778	34.732	1.012	27.825	206	139	465
-1919	34.725	0.873	27.827	206	99	-
-2246	34.707	0.594	27.836	208	76	473

TABLE 1. (continued)

Depth, m	Salinity, ppt	Tpot, °C	σ_θ	O_2, µmol kg^{-1}	Ba, pmol kg^{-1}	pCO_2, µatm
			Station 76 (continued)			
-2527	34.556	0.377	27.84	210	425	476
-2808	34.699	0.199	27.84	214	115	478
-3089	34.685	0.035	27.847	217	160	-
-3744	34.681	-	27.85	229	105	476
-4025	34.661	-	27.857	235	160	467
			Station 78: 61°45' S, 76°16' E ; Water Column, 3951 m			
-10	33.699	1.447	26.963	349	1471	282
-20	33.701	1.442	26.962	349	1250	280
-35	33.805	1.389	26.97	348	2240	-
-75	33.039	-1.542	27.381	307	149	387
-100	34.312	-0.213	27.496	251	190	466
-200	34.576	1.77	27.646	178	569	602
-300	34.634	1.882	27.699	174	432	-
-400	34.687	1.885	27.726	177	342	567
-500	34.699	1.861	27.743	181	374	538
-600	34.716	1.816	27.758	185	-	-
-700	34.728	1.735	27.773	192	278	512
-800	34.734	1.681	27.785	192	254	493
-900	34.737	1.574	27.795	195	224	501
-1100	34.739	1.398	27.809	199	201	491
-1300	34.514	1.203	27.819	203	324	467
-1500	34.731	1.04	27.83	204	124	487
-1750	34.719	0.806	27.835	205	130	492
-2000	34.703	0.602	27.831	206	147	485
			Station 79: 64°10' S, 84°02' E; Water Column, 3628 m			
-10	33.795	0.979	27.053	346	3646	296
-39	33.868	0.479	27.161	339	8272	302
-68	34.204	-1.679	27.556	297	189	392
-88	34.287	-1.597	27.594	295	119	409
-117	34.323	-1.559	27.640	296	189	392
-147	34.356	-1.414	27.650	296	130	400
-171	34.373	-1.398	27.658	285	151	-
-195	34.394	-1.234	27.670	274	193	391
-244	34.476	-0.297	27.711	253	176	460
-293	34.544	1.210	27.742	198	315	536
-399	34.690	1.285	27.767	199	300	-
-481	34.708	1.266	27.786	200	261	-
-577	34.724	1.166	27.800	203	308	506
-673	34.728	1.116	27.810	203	200	-
-770	34.717	1.031	27.816	205	187	-
-866	34.730	0.908	27.818	207	201	483
-962	34.714	0.846	27.822	207	181	504
-1100	34.707	0.775	27.826	207	179	-
-1200	34.704	0.696	27.829	207	227	483
-1300	34.701	0.624	27.831	207	157	495
-1359	34.686	0.545	27.834	208	180	-
-1457	34.697	0.462	27.836	209	132	489
-1554	34.694	0.387	27.836	210	150	490
-1651	34.699	0.324	27.837	211	163	-
-1748	34.687	0.267	27.839	212	217	488
-1942	34.683	0.156	27.842	214	113	499
-2330	34.676	-0.015	27.845	218	121	503
-2670	34.673	-0.155	27.851	222	118	494
-3107	34.677	-0.325	27.858	231	103	476
-3399	34.677	-0.413	27.861	236	181	463

TABLE 1. (continued)

Depth, m	Salinity, ppt	Tpot, °C	σ_θ	O_2, µmol kg^{-1}	Ba, pmol kg^{-1}	pCO_2, µatm
		Station 81: 65°59' S, 67°16' E; Water Column, 3098 m				
-10	34.143	0.295	27.382	340	114	358
-25	34.146	0.266	27.386	340	49	357
-50	34.320	-1.442	27.618	313	91	392
-75	34.413	-1.633	27.701	292	108	445
-100	34.428	-1.646	27.715	290	110	370
-200	34.503	-0.983	27.745	272	109	404
-300	34.620	0.227	27.787	232	248	452
-400	34.670	0.763	27.802	215	283	477
-500	34.678	0.715	27.822	214	280	484
-600	34.688	0.758	27.819	211	225	486
-700	34.688	0.660	27.819	212	236	476
-800	34.699	0.669	27.826	210	214	495
-900	34.697	0.619	27.822	209	178	488
-1000	34.697	0.550	27.827	209	181	-
-1100	34.698	0.483	27.831	209	215	496
-1300	34.690	0.363	27.841	210	145	-
-1500	34.688	0.221	27.845	213	176	469
-1750	34.687	0.091	27.844	216	171	455
-2000	34.687	-0.018	27.847	219	135	-
		Station 86: 63°45' S, 41°59' E; Water Column, 4688 m				
-10	33.858	0.821	27.136	339	32	347
-25	33.854	0.81	27.137	339	113	367
-35	33.864	0.74	27.147	338	195	359
-50	33.873	0.644	27.343	332	164	346
-75	34.195	1.607	27.51	318	31	344
-100	34.335	0.123	27.597	253	155	472
-200	34.645	1.441	27.727	186	543	569
-300	34.684	1.421	27.764	189	207	557
-400	34.705	1.401	27.785	193	361	532
-500	34.714	1.3	27.798	196	341	526
-600	34.721	1.195	27.799	198	216	517
-700	34.723	1.076	27.811	201	186	-
-800	34.719	0.959	27.819	203	171	-
-900	34.713	0.846	27.822	204	292	513
-1000	34.71	0.752	27.825	205	537	-
-1100	34.705	0.658	27.829	206	246	494
-1300	34.696	0.48	27.833	208	120	500
-1500	34.693	0.344	27.836	209	100	494
-1750	34.686	0.225	27.839	210	144	503
-2000	34.683	0.106	27.844	215	130	494
		Station 87: 65°10' S, 32°01' E; Water Column, 4584 m				
-10	33.857	1.057	27.123	340	58	347
-30	33.946	0.76	27.19	339	119	-
-50	34.239	-1.525	27.535	328	61	343
-75	34.314	-1.397	27.61	307	62	376
-100	34.411	-0.678	27.662	265	83	448
-200	34.659	1.366	27.747	190	367	543
-300	34.683	1.268	27.773	195	212	523
-400	34.696	1.165	27.79	199	156	520
-500	34.701	1.125	27.798	201	260	521
-600	34.713	1.035	27.813	201	115	502
-700	34.714	0.941	27.822	203	191	501
-800	34.709	0.762	27.826	204	157	-
-900	34.701	0.722	27.826	206	116	479
-1000	34.698	0.592	27.829	207	147	-

TABLE 1. (continued)

Depth, m	Salinity, ppt	Tpot, °C	σ_θ	O_2, µmol kg^{-1}	Ba, pmol kg^{-1}	pCO_2, µatm
			Station 87 (continued)			
-1100	34.695	0.505	27.832	208	128	494
-1300	34.688	0.347	27.836	209	146	479
-1500	34.679	0.224	27.835	213	96	473
-1750	34.677	0.079	27.841	215	146	493
-2000	34.673	-0.063	27.834	219	118	487
			Station 88: 61°01' S, 32°17' E; Water Column, 5189 m			
-10	33.786	1.305	27.049	342	319	315
-40	33.788	1.119	27.064	342	384	314
-70	33.915	-1.042	27.319	341	37	342
-90	34.013	-1.425	27.400	338	85	354
-120	34.162	-1.019	27.473	308	136	397
-150	34.313	0.314	27.585	243	233	497
-175	34.439	0.794	27.630	220	406	-
-200	34.565	1.293	27.677	196	535	557
-250	34.627	1.431	27.717	189	492	-
-300	34.650	1.448	27.734	188	337	556
-400	34.681	1.425	27.761	190	327	561
-500	34.706	1.371	27.785	193	261	527
-600	34.712	1.281	27.796	197	302	529
-700	34.714	1.168	27.806	199	263	499
-800	34.715	1.046	27.814	201	357	-
-900	34.711	0.911	27.820	203	276	509
-1000	34.707	0.802	27.824	204	230	-
-1150	34.701	0.636	27.829	206	230	482
-1300	34.695	0.494	27.833	208	196	496
-1500	34.688	0.334	27.836	209	222	496
-1700	34.682	0.224	27.838	210	142	509
-1900	34.678	0.133	27.839	214	<4	503
-2150	34.682	0.013	27.849	217	46	471
-2400	34.680	-0.095	27.853	220	109	-
-2700	34.667	-0.206	27.849	225	67	-
-3000	34.666	0.303	27.853	229	67	-
-3300	34.664	-0.389	27.855	232	81	-
-3700	34.662	0.488	27.857	237	73	454
-4100	34.658	-0.570	27.857	240	83	446
-4500	34.655	-0.639	27.858	242	45	454
			Station 89: 56°59'S, 31°50' E; Water Column, 5426 m			
-10	33.939	2.847	27.055	326	50	352
-30	33.948	1.908	27.142	333	93	337
-50	33.965	1.867	27.156	335	53	355
-75	33.983	1.411	27.205	332	135	353
-100	34.026	-0.015	27.328	332	189	369
-200	34.298	1.136	27.483	241	355	516
-300	34.506	1.882	27.617	180	398	617
-400	34.608	1.763	27.681	180	415	584
-500	34.672	1.718	27.72	181	291	571
-600	34.694	1.689	27.748	185	286	546
-700	34.72	1.635	27.766	189	295	536
-800	34.746	1.541	27.782	193	259	-
-900	34.73	1.399	27.796	196	194	505
-1000	34.731	1.299	27.803	198	251	-
-1100	34.737	1.196	27.811	200	224	-
-1300	34.726	0.975	27.823	204	244	496
-1500	34.722	0.729	27.827	206	177	505
-1750	34.7	0.497	27.832	208	142	487
-2000	34.701	0.324	27.838	210	157	483

Station 90: 53°01' S, 31°13' E; Water Column, 5260 m

-10	33.947	3.854	26.961	323	94	353
-30	33.953	3.645	26.985	326	385	354
-50	33.989	2.046	27.135	330	220	355
-75	34.032	1.422	27.234	325	140	383
-100	34.045	1.219	27.264	321	200	361
-200	34.237	1.061	27.429	257	575	499
-300	34.487	1.882	27.571	179	412	588
-400	34.533	1.683	27.623	182	291	598
-500	34.617	1.898	27.674	173	184	566
-600	34.640	1.764	27.703	176	200	576
-700	34.673	1.784	27.725	178	223	-
-800	34.701	1.789	27.747	183	201	-
-900	34.722	1.773	27.768	188	122	527
-1000	34.731	1.700	27.779	192	202	-
-1100	34.738	1.626	27.792	194	166	494
-1300	34.738	1.431	27.806	198	131	486
-1750	34.718	0.876	27.824	205	137	483
-2000	34.708	0.577	27.832	208	127	-

Station 95: 47°09' S, 23°34' E; Water Column, 5559 m

-10	33.873	6.868	26.551	298	89	362
-30	33.879	6.769	26.569	298	105	367
-50	33.884	6.526	26.608	300	76	363
-75	33.897	6.2	26.658	301	88	358
-100	33.951	5.216	26.821	303	95	371
-200	34.095	4.346	27.032	286	176	403
-300	34.186	3.737	27.167	267	206	452
-400	34.183	3.22	27.215	260	209	440
-500	34.205	2.847	27.266	247	279	464
-600	34.264	2.632	27.332	226	249	557
-700	34.332	2.613	27.388	209	180	57
-800	34.98	2.571	27.444	185	220	-
-900	34.46	2.503	27.5	185	153	596
-1000	34.516	2.466	27.547	182	139	-
-1100	34.571	2.429	27.595	179	111	563
-1300	34.659	2.417	27.666	180	167	573
-1500	34.712	2.358	27.713	186	148	560
-1750	34.765	2.213	27.768	197	123	-
-2000	34.786	1.898	27.802	204	69	478

Station 98: 38°00' S, 23°18' E; Water Column, 5370 m

-10	35.487	23.056	24.291	213	384	331
-30	35.499	22.228	24.537	216	1174	330
-50	35.539	21.808	24.685	212	571	332
-75	35.566	21.256	24.858	209	268	-
-100	35.552	20.345	24.74	196	402	362
-200	35.609	17.576	25.845	213	145	362
-300	35.469	15.557	26.212	199	189	395
-400	35.328	14.058	26.431	208	216	397
-500	35.196	12.929	26.561	208	208	407
-600	35.024	11.683	26.67	214	89	414
-700	34.884	10.463	26.779	210	110	439
-800	34.745	9.096	26.899	204	98	-
-900	34.607	7.57	27.031	196	129	503
-1000	34.527	6.487	27.111	197	368	-
-1100	34.448	5.425	27.19	198	180	536
-1300	34.428	3.917	27.342	190	138	572
-1500	34.543	3.418	27.483	169	127	611
-1750	34.6	2.724	27.592	177	134	589

Station 99: 37°59' S, 30°01' E; Water Column, 4129 m

-10	35.682	21.711	24.821	219	59	330
-30	35.68	21.721	24.819	220	23	324

TABLE 1. (continued)

Depth, m	Salinity, ppt	Tpot, °C	σ_θ	O_2, μmol kg^{-1}	Ba, pmol kg^{-1}	pCO_2, μatm
			Station 99 (continued)			
-50	35.681	21.714	24.822	220	37	326
-75	35.605	19.894	25.255	217	77	338
-100	35.615	18.914	25.516	209	92	347
-200	35.62	16.996	25.993	224	142	346
-300	35.615	16.835	26.028	226	92	337
-400	35.418	15.1	26.274	206	147	388
-500	35.234	13.521	26.47	216	126	389
-600	35.116	12.463	26.59	214	177	414
-700	34.978	11.298	26.702	212	128	-
-800	34.824	10.042	26.81	211	122	445
-900	34.719	8.835	26.918	203	114	-
-1000	34.602	7.492	27.038	193	145	522
-1100	34.501	6.371	27.113	198	89	530
-1300	34.385	4.247	27.273	203	162	546
-1500	34.493	3.627	27.423	178	165	538
-1750	34.592	2.964	27.565	171	138	617

(-, no data)

energy dispersive X-ray detector, using an automatic particle recognition program [Raeymakers, 1986; Storms, 1988]. Barite is observed to occur as discrete particles with log-normal size distributions, having their modes at 1 and 0.84 μm, respectively. Smallest crystals recorded are 0.32 μm at 500 m and 0.08 μm at 700 m. The barium quantities carried by the detected barite crystals, normalized to unit volume, were compared with those obtained by ICP-OES. This comparative study shows that 81% (at 700 m) to 86% (at 500 m) of the total barium is carried by barite microcrystals, thus confirming earlier results [Dehairs et al., 1980]. This good agreement between barite and total barium is also consistent with the high barium to aluminum ratio we observe in total suspended matter (these Al data are reported by Poisson et al. [1990]) relative to crustal material. This indicates that excess barium is present which is not carried by the aluminosilicate fraction in the suspended matter.

DISCUSSION

For some of the stations given in Table 1, particulate barium profiles are compared with profiles of dissolved oxygen and CO_2 partial pressure (Figure 2). From Table 1 and Figure 2, it appears that for the stations south of the Polar Front, barium maxima occur within the oxygen minimum or above it, in the gradient leading towards the oxygen minimum. However, some of these stations (78, 79, 98) show also very high barium values in the euphotic layer, eventually exceeding the barium maximum associated with the oxygen minimum. Moreover, in some isolated cases, deepwater barium peaks do occur. These often coincide with increased concentrations of particulate Ca, Sr, and Si (data reported by Poisson et al. [1990]). We tentatively explain such deepwater maxima to result through the occasional disintegration of large, fast settling carrier particles en route to the sediments and which thereby inject their load of small particles into the deep water column.

Next we will focus the discussion on the occurrence of the barium maxima in the euphotic layer and in the oxygen minimum layer.

The Barium Maximum in the Region of the Oxygen Minimum and pCO_2 Maximum

For all stations between the Polar Front and the Antarctic Divergence, the oxygen minimum and pCO_2 maximum are located between 200 and 500 m depth. The barium maximum is located in the same depth interval, but peak values do not always coincide. Neither the oxygen minimum nor the barium maximum is located on isopycnal surfaces. In the oxygen minimum, σ_θ decreases from south to north (e.g., station 87, 65°11'S, σ_θ = 27.747; station 94, 50°35'S, σ_θ = 27.657). Oxygen saturation values in the oxygen minimum fit into a very narrow range (from 346 to 352 μM), while this range is wider for oxygen saturation values taken along isopycnal surfaces (e.g., σ_θ = 27.700; oxygen saturation between 347 and 371 μM). These observations suggest a common origin for the oxygen minimum waters and also suggest water movement, to some degree, to occur diapycnally.

The highest values for oxygen in the oxygen minimum and the lowest values for barium in the barium maximum are found at the southernmost stations. Between 65°S and 55°S oxygen decreases northward, while barium and pCO_2 decrease southward. In Figure 3 we plot barium, integrated between 200 and 700 m (that is the depth region in which the maximum is located) versus the dissolved oxygen content in the oxygen minimum for the stations located between the divergence and the Polar

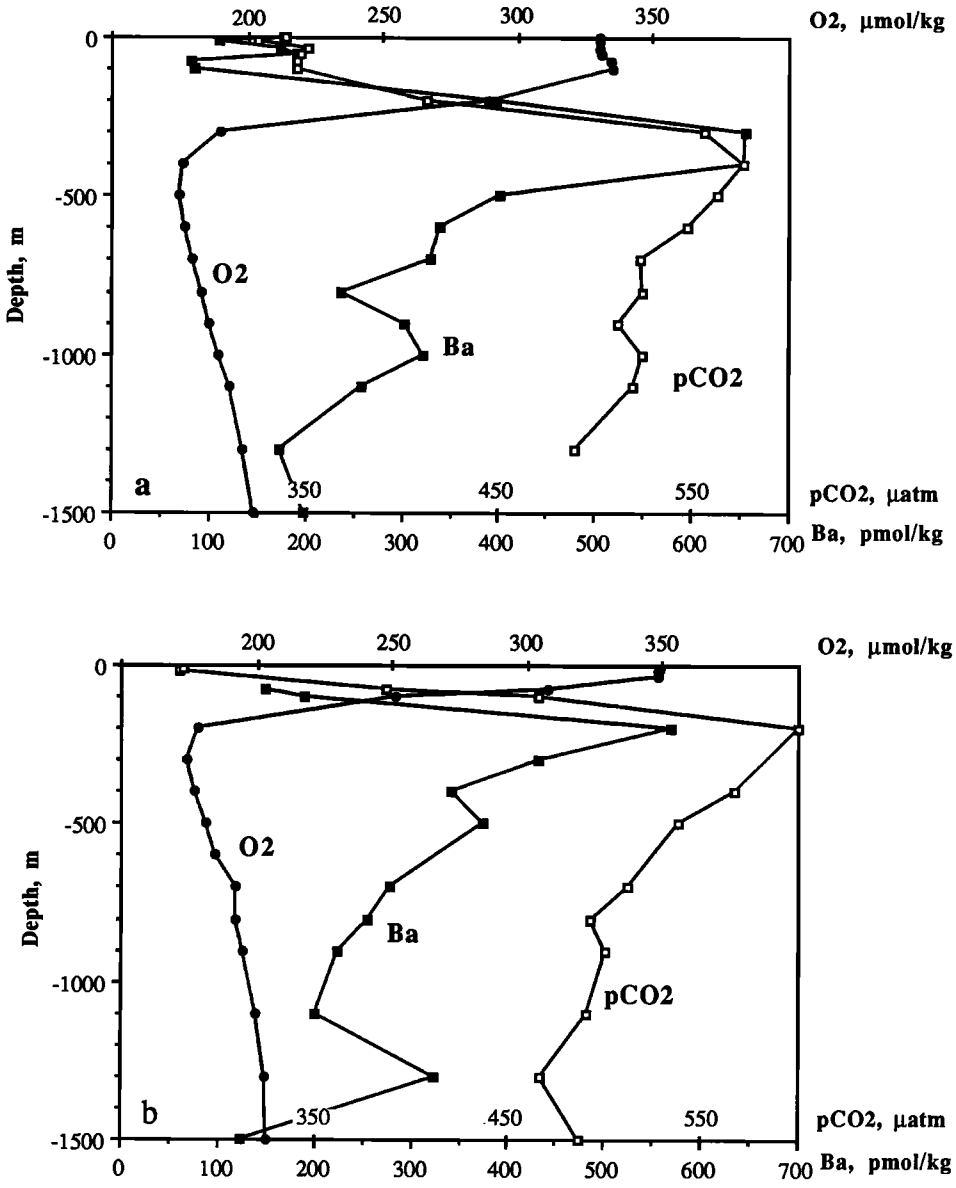

Fig. 2. Vertical profiles of particulate barium (solid squares, pmol kg^{-1}), dissolved oxygen (solid circles, µmol kg^{-1}) and pCO_2 (open circles, µatm) at stations (a) 75, (b) 78, (c) 87, and (d) 99. For station 78 the surface water Ba maximum (Ba > 1000 pmol kg^{-1}; see Table 1) is not shown.

Front. A significant correlation is apparent ($r = 0.82$; $p < 0.01$), showing increased barium-barite content for increasing oxygen consumption.

However, this observed relationship between oxygen and barium appears to hold only for the stations south of the Polar Front. Stations 95, 98, and 99 located north of the Polar Front do not fit it, showing lower Ba concentrations than predicted by the Ba - O_2 relationship (Figure 3). For the stations located within the Antarctic Circumpolar Current, the observations suggest some causal relation between consumption of oxygen due to heterotrophic activity and production, or rather release, (as discussed below) of barite crystals. They also suggest the oxygen minimum waters to flow north-northeastward, away from the divergence. This is also emphasized by the following observations.

1. For the region south of the Polar Front the general south to north- northeast decrease of oxygen in the oxygen minimum is paralleled by an increase of nitrate in the nitrate maximum layer (generally located slightly above the oxygen minimum; nitrate data are reported by Poisson et al. [1990]), with oxygen and nitrate

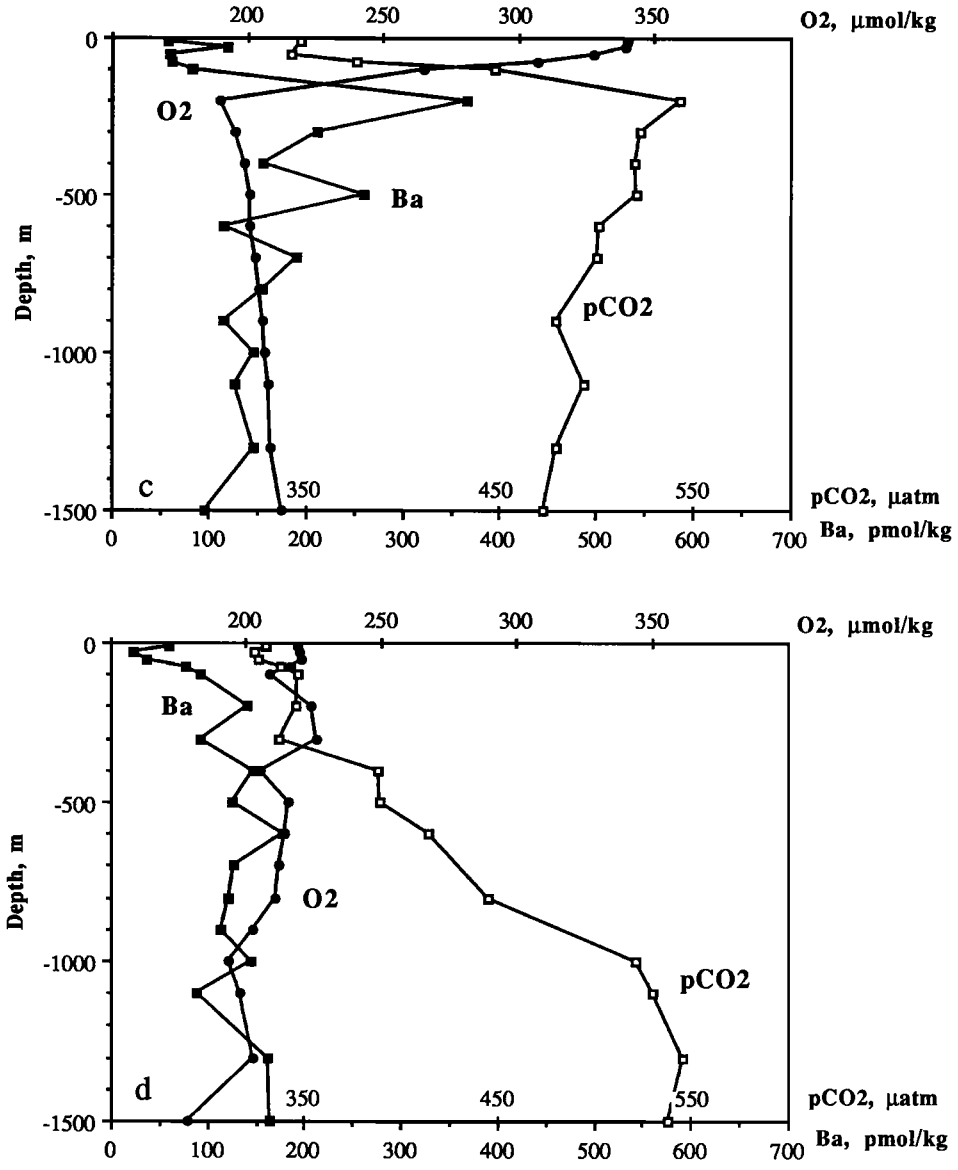

Fig. 2. (continued)

significantly correlated (Figure 4). The slope of this relationship (ΔO_2 / ΔNO_3) is |7.2|, which is close to the Redfield ratio of 8.6 [Redfield et al., 1963]. For the area investigated here, we believe it is not realistic to inspect for oxygen consumption along isopycnal surfaces, due to the sharp upward bending of the isopycnals as they approach the divergence. Indeed, in such a situation the effect due to the oxidation of organic matter transported by advection along an isopycnal surface is likely to be expressed at a different depth than the effect due to the oxidation of organic matter carried by the large, vertically settling particles. We also inspected the O_2 / NO_3 relationship along isopycnal surfaces (σ_θ 27.600 and 27.700) encompassing the oxygen minimum. In this case the correlations are less significant, and ΔO_2 / ΔNO_3 ratios are ≥ |20|. This is much in excess of values observed along isopycnal surfaces in the Atlantic, Indian, and Pacific oceans (ΔO_2 / ΔNO_3 = |11| [Takahashi et al., 1985; Broecker et al., 1985; Peng and Broecker, 1987]).

2. As was stated above, the Ba-oxygen relationship holds only for stations located within the Antarctic Circumpolar Current. North of the Polar Front the oxygen minimum occurs much deeper (> 1400 m) in the water column, and values of the Ba maximum are smaller than expected from the described Ba-O_2 relationship. This indicates the Ba maximum in the circumpolar current to be a local phenomenon reflecting

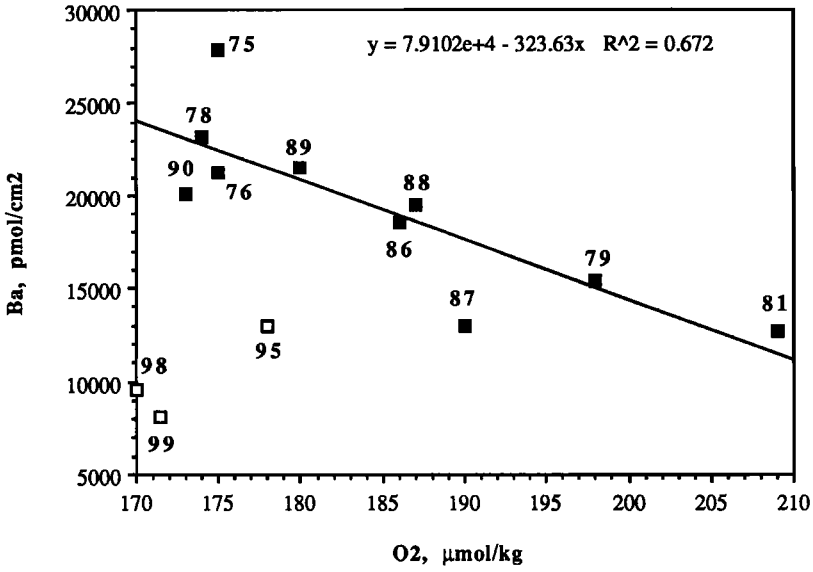

Fig. 3. Particulate barium (pmol cm^{-2}), integrated over the barium maximum versus dissolved oxygen (µmol kg^{-1}) in the oxygen minimum for stations south of the Polar Front.

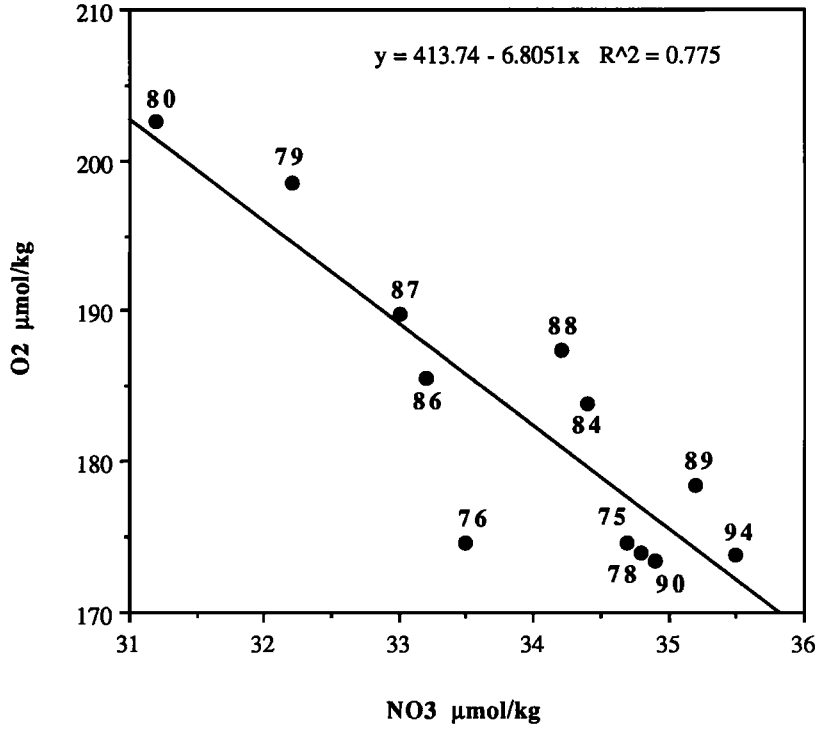

Fig. 4. Dissolved oxygen (µmol kg^{-1}) in the oxygen minimum versus nitrate (µmol kg^{-1}) in the nitrate maximum for stations south of the Polar Front.

the particular properties of this water mass. Indeed, if both the Ba maximum and the oxygen minimum were properties advected from the adjacent oceanic basins towards the divergence, the Ba maximum north of the Polar Front should be as high or higher than south of the front; this is not observed.

The similarity between the observed stoichiometry of nitrate and oxygen in the oxygen minimum region with

that predicted by Redfield ratio values, and the discontinuity in the values of the barium maximum across the Polar Front suggest that water in the oxygen minimum layer (i.e. the 200-500 m depth layer) increases in age in a general north- northeastward direction. We believe our conclusions are also supported by Toggweiler et al.'s [1989] observations indicating that water upwelling at the divergence is largely Circumpolar Water containing relatively little deep water from the major basins to the north.

In the following we check whether the decrease of oxygen in the oxygen minimum over a given distance is compatible with known rates of primary production. Therefore we will follow a parcel of water in the oxygen minimum layer from the source region to some point located downstream in the circumpolar current. We choose station 87 as the source region since it is located upstream, close to the Antarctic Divergence. Stations 78, 76, and 75, located to the northeast and downstream of station 87, are choosen to represent the target region. For the circumpolar current, along the prime meridian, Whitworth and Nowlin [1987] calculated geostrophic speeds between 2 and 10 cm s^{-1} at 200 m depth. Taking a speed of 5 cm s^{-1} it is calculated that the distance between stations 87 and 78 (2500 km) is covered in 580 days and between stations 87 and 76,75 (2000 km) in 460 days. For a 200 m depth interval, centered on the oxygen minimum depth, the differences in integrated oxygen content between station 87 (the source) and stations 78, 76, and 75 (the target) amount to 3400 mmol O_2 m^{-2} (87 to 78) and 4100 mmol O_2 m^{-2} (87 to 76, 75). Taking into account the calculated transit time for the oxygen minimum water, these observed oxygen deficits reflect oxygen utilization rates of 5.9 mmol m^{-2} d^{-1} (87 to 78) and 8.9 mmol m^{-2} d^{-1} (87 to 76,75). These oxygen consumptions are equivalent to the oxidation respectively of 4.3 and 6.5 mmol C m^{-2} d^{-1}, using the ΔO_2 / ΔC Redfield ratio (175 / 127) from Takahashi et al. [1985] and Peng and Broecker [1987]. If we assume these rates of organic carbon oxidation to represent the totality of new production, itself representing 45% of total production in the Antarctic [Eppley and Peterson, 1979], we calculate yearly averaged daily total productions of 115 and 173 mg C m^{-2} d^{-1}; this is equivalent to yearly productions of 42 and 63 g C m^{-2} yr^{-1}. These values will be compared with known rates of primary production. From the discussion on global maps of primary productivity given by Berger [1989], values for the southern ocean appear to range between 60 and 125 g C m^{-2} yr^{-1}. Recent seasonal primary production rates for the open southern ocean range from 100 to 350 mg C m^{-2} d^{-1} ([e.g., Wefer et al., 1982; Le Jehan and Tréguer, 1983; Lancelot et al., 1989], but occasional high values up to 2000 mg C m^{-2} d^{-1} have been observed in the area of the Antarctic Peninsula [Bodungen et al., 1986]. Taking the production period to last during 4 months of the year, these seasonal productivities translate into annual productivities ranging from 12 to 43 g C m^{-2} y^{-1}, without considering the extreme value reported for the peninsula region. It appears that our calculated values are similar to the values deduced from global maps and to the higher values reported for seasonal primary productivity. These comparisons indicate that the observed difference in oxygen content of the oxygen minimum layer between station 87 and stations 78, 76, and 75 is consistent with the described general flow pattern of the oxygen minimum water.

It remains to be checked whether the estimated aging of the water in the oxygen minimum layer is also consistent with the observed accumulation of barite. Without considering the dissolution effect and assuming Stokes sedimentation law to apply, a 1-μm large barite crystal will need about 5 years to cross a 200-m-thick water layer (what is about the width of the subsurface barium maximum layer). Furthermore, barite dissolution in seawater is a slow process with a dissolution rate estimated at 0.075 μm yr^{-1} [Dehairs, 1979; Dehairs et al., 1980]. Thus barite residence time in the oxygen-minimum region can exceed the estimated aging of the water between considered source and target regions.

From the preceding discussion it appears that there is evidence for internal consistency between evolution of the oxygen minimum layer over a given distance as controlled by advection velocity and primary production on one hand, and accumulation of barite as controlled by sedimentation and dissolution on the other. Barite content thus reflects and integrates former biological processes.

Origin of the Oxygen Minimum

We propose the following scenario for the origin of the oxygen minimum, pCO_2 maximum in the Antarctic Circumpolar Current. This origin is likely to be upwelling along the Antarctic Divergence. At the divergence (southernmost stations 80 and 81) the minimum oxygen value is 209 μM at 900 to 1000 m depth, at σ_θ = 27.83. For all other stations between the divergence and the Polar Front, the 204 to 209 μM oxygen range is found at the same isopycnal surface (σ_θ between 27.83 and 27.84) but deeper (i.e., below the salinity maximum) than at stations 80 and 81 (Figure 5). This suggests the occurrence of the 209 μM value as a minimum at stations 80 and 81 to be induced through southward advection of deep water. It seems thus likely that deep water with a low oxygen value (i.e., the 209 μM value) is originally advected to the south, rising to shallower depths along the 27.83 isopycnal surface. From the divergence onward the water carrying this oxygen value returns to the north and northeast. Its oxygen content is then affected by local processes of oxygen consumption which enhance the oxygen minimum. This scenario is also supported by the data for freon 11 and 12 [Mantisi, 1989; Poisson et al., 1990]. Freon concentrations in the oxygen minimum layer increase from the vicinity of the divergence to the north and northeast. This increasing contamination of the upwelled, freon-poor, deep water with distance from the divergence, suggests that the oxygen minimum waters are flowing away from the divergence and accumulate the freon that is penetrating from the surface layers.

The Barium Maximum in the Euphotic Zone

Barium concentrations in the euphotic layer can rise occasionally to high values. For stations 78 and 79 these maxima greatly exceed (respectively by a factor of 4 and

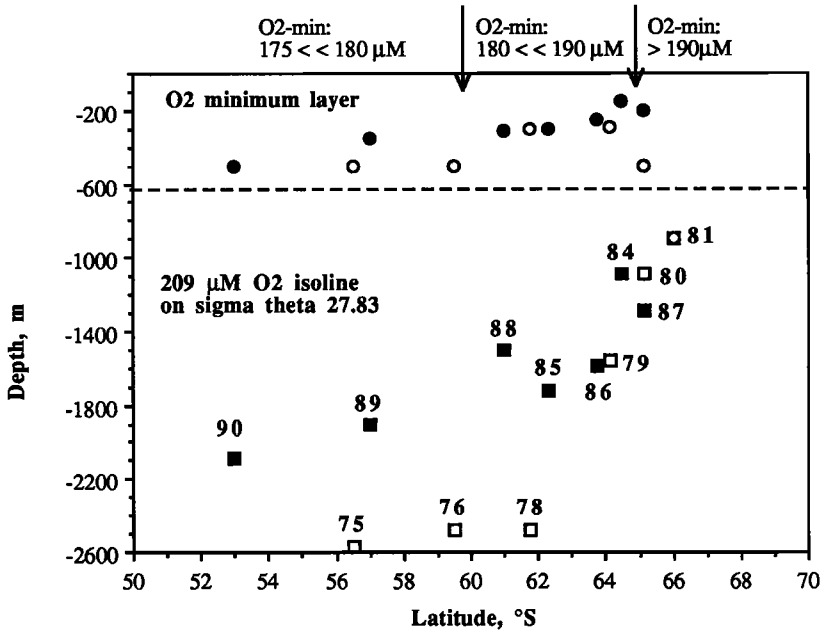

Fig. 5. Meridional section between 53°S and 66°S showing the depths at which the 209 µM oxygen value (squares) and the oxygen minimum (circles) are located. Solid symbols, along 30°E; open symbols, along 84° E.

20)-those in the oxygen minimum layer. As shown in Figure 6, they coincide with higher chlorophyll-*a* concentrations (1.1 to 1.2 µg L^{-1} [Goffart and Hecq, 1988]), as compared to other stations (< 0.5 µg L^{-1}) and the nitrate values in the surface waters are lower (station 78; 21.3 µmol L^{-1}; station 79; 23.5 µmol L^{-1}) than at other stations (typically 25 to 27 µmol L^{-1}). For station 80 no particulate matter was sampled, but the high Chl-*a*

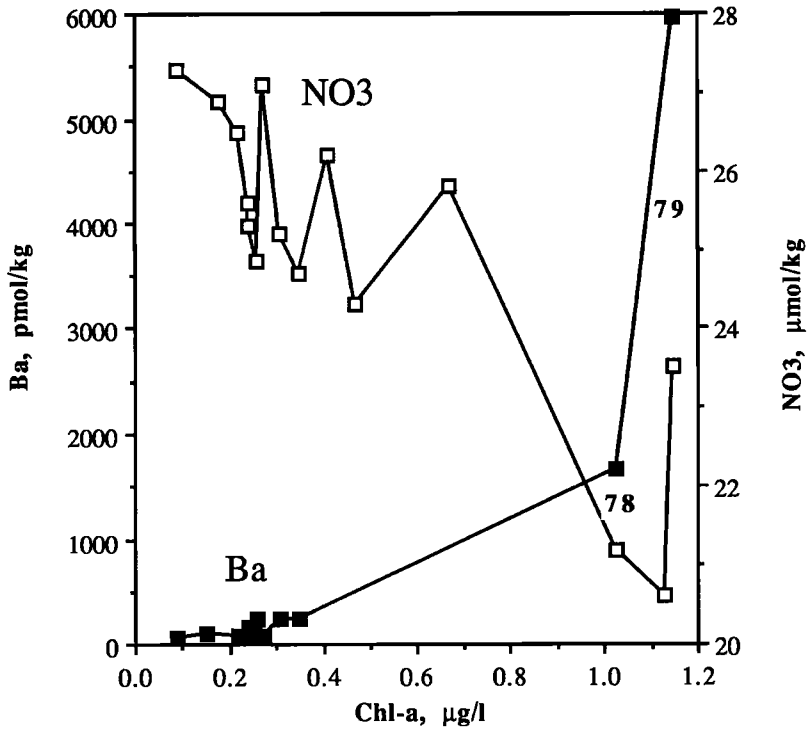

Fig. 6. Particulate barium (solid squares, pmol kg^{-1}) and nitrate (open squares, µmol kg^{-1}) versus Chl-*a* (µg L^{-1}) in the surface waters (<50 m).

and the low nitrate values in the euphotic layer suggest that here also high barium concentrations were present.

This coincidence of high barium values with high chlorophyll-*a* values suggests active production of barite. However, it is also possible that the higher phytoplankton biomass present sustains a higher biomass and activity of heterotrophs. This is suggested by the observed positive relationship between the ammonium mineralization rate and the barium content in the euphotic layer at other stations (Figure 7). Since for stations 78 and 79 no mineralization rates were measured, we do not know whether the observed relationship with barium applies also for these sites with extreme barium contents in the euphotic layer. Bacterial biomass, estimated from countings on acrydine-orange stained samples obtained during the same cruise [Dezan, 1987; Joiris et al., 1988], is not significantly higher at station 78 (1.6 μg C L^{-1}), but it is at stations 79, 80, and 81 (respectively 2.5; 5.1 and 4.3 μg C L^{-1}). However, for station 81 this high bacterial biomass does not coincide with a high barium content.

Finally, SEM-EMP data for the -10 m sample at station 76 show barite to occur mainly as small crystals (<0.5 μm) forming aggregates associated with larger particles composed of mixed biogenic debris including diatom tests. This observation is in favor of passive barite formation within microenvironments, composed here of mixed aggregates of organic detritus and biogenic debris.

Although these facts do not give clear-cut evidence, the majority of the observations is in favor of passive production of barite in the euphotic layer. They also indicate that there is a time lag between the observed phenomena in the oxygen minimum layer and the euphotic layer. Indeed, biological activity, which is responsible for the extreme barium content in the euphotic layer at station 79 (Table 1), did not yet have any impact on the barium content in the oxygen-minimum area at the time of sampling, as evidenced by the low Ba value in the subsurface barium maximum at this station.

The Production and Redistribution of Barite

From the SEM-EMP investigations in this study, it appears that in the surface waters barite is associated with composite biogenic aggregates, while at greater depths barite crystals occur as free particles. SEM-EMP investigations on samples we took during a more recent southern ocean cruise (EPOS-2; November-December 1988; Scotia-Weddell Confluence area), also showed occurrence of large (>100, <1000 μm), loosely packed bioaggregates carrying barite crystals. Such aggregates were abundant in the first 200 m of the water column but virtually absent below. These observations are very much in accord with those made by Bishop [1988] showing, for surface waters in the NW and SE Atlantic Ocean, total Ba to be associated with the size fraction > 53 μm. At 100 to 200 m depth the largest fraction of barium is seen to shift toward the < 53 μm size class [Bishop, 1988].

These observations suggest that mixed biogenic aggregates represent the microenvironments where barite microcrystals are formed. These aggregates settle out of the mixed layer but are disintegrated just below the first

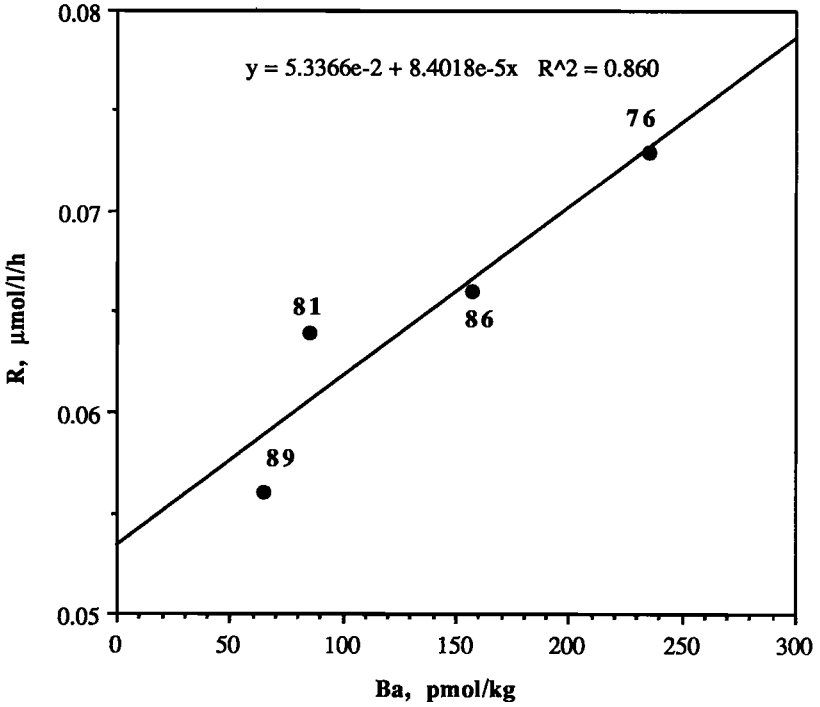

Fig. 7. Mineralization rate of ammonia (μmol L^{-1} h^{-1}) versus particulate barium (pmol kg^{-1}) content in the surface waters (<50 m).

few hundred meters of depth, setting free the micron-sized barite crystals they carry. These discrete barite particles will now accumulate as a result of their small settling and dissolution rates. At the Ba maximum depth, barite content is no longer related to instantaneous biological activity, as it probably is in the euphotic layer, but rather reflects former biological activities.

The possibility that barite forms in situ at the Ba maximum depth as a result of in situ bacterial activity seems unlikely. Indeed, instantaneous heterotrophic activity, as reflected by the measured ammonium mineralization rates, is inversely correlated with Ba at these depths. Here oxygen content seems to control mineralization rates as indicated by the positive correlation we observe between both parameters.

CONCLUSIONS

The distribution of particulate Ba in surface waters of the mixed layer is closely linked to the biological activity. At depth, the coincidence of the Ba-barite maximum with the oxygen minimum and the inverse correlation between these extremes point towards a significant, local, biological control on the oxygen minimum. The identification of biological activity, besides advection, as a main process controling the oxygen minimum has set constraints as to the flow direction of these oxygen minimum waters. These waters appear to be originally advected to the south as oxygen poor deep waters. They well up at the Antarctic Divergence from where they spread out partly to the north-northeast. From then on, oxidation of settling organic matter, produced in local surface waters, consumes oxygen and induces an oxygen minimum. The distribution of pCO_2 in this region is the mirror distribution of O_2 and therefore also reflects the combined effect of physical, chemical and biological processes. The situation described is probably typical for the area between the Antarctic Divergence and the Polar Front.

While the data presented here again highlight the link between barite and biological activity, which is essential in the study of the carbon cycle, they also reveal the important role of biogenic microenvironments, either as formation sites of barite, or as carriers of barite to the deeper layers, thereby lending strong support to the original Chow and Goldberg [1960] model.

Acknowledgments. We are grateful to H. Neybergh, at the Belgian Geological Survey, for providing access to the ICP-OES equipment in his laboratory and assistance during the measurements. We thank M. Pamatmat for his comments and discussions. The crew of the *Marion Dufresne* as well as the TAAF administration are thanked for their logistical support. This research is part of the "Belgian Scientific Research Programme on Antarctica -- Phase 1" (Prime Minister's Services, Science Policy Office). The scientific responsibility is assumed by its authors. F.D. is a research associate at the National Fund for Scientific Research, Belgium.

REFERENCES

Armstrong, F. A. I., C. R. Steins and J. D. H. Strickland, The measurement of upwelling and subsequent biological processes by means of the Technicon autoanalyzer and associated equipment, *Deep Sea Res.*, *14*, 381-389, 1967.

Arrhenius, G., and E. Bonatti, Neptunism and vulcanism in the ocean, in *Progress in Oceanography*, vol. 3, edited by M. Sears, pp. 7-22, Pergamon, New York, 1965.

Berger, W. H., Global maps of ocean productivity, in *Productivity of the ocean: Present and Past, Dahlem Workshop Reports, Life Sci. Res. Rep. 44*, edited by W.H. Berger, V.S. Smetacek, and G. Wefer, pp. 429-455, John Wiley, New York, 1989.

Bishop, J. K. B., The barite-opal-organic carbon association in oceanic particulate matter, *Nature*, *332*, 341-343, 1988.

Bishop, J. K. B., Regional extremes in particulate matter composition and flux: Effects on the chemistry of the ocean interior, in *Productivity of the ocean: Present and Past, Dahlem Workshop Reports, Life Sci. Res. Rep. 44*, edited by W.H. Berger, V.S. Smetacek and G. Wefer, pp. 117-137, John Wiley, New York, 1989.

Bishop, J. K. B., and J. M. Edmond, A new large volume filtration system for the sampling of oceanic particulate matter, *J. Mar. Res.*, *34*, 181-198, 1976.

Bodungen, B. v., V. S. Smetacek, M. M. Tilzer, and B. Zeitschel, Primary production and sedimentation during spring in the Antarctic Peninsula region, *Deep Sea Res.*, *33*, 177-194, 1986.

Broecker, W. S., T. Takahashi, and T. T. Takahashi, Sources and flow pattern of deep-ocean waters as deduced from potential temperature, salinity and initial phosphate concentrations, *J. Geophys. Res.*, *90*, 6925-6939, 1985.

Brook, A., A. Fotheringham, J. Bradley, and A. Jenkins, Barium accumulation by desmids of the genus *Closterium* (Zygnemaphyceae), *Br. Phycol. J.*, *15*, 261-264, 1980.

Burman, J.-O., C. Pontér, and K. Boström, Metaborate digestion procedure for inductively coupled plasma--optical emission spectrometry, *An. Chem.*, *50*, 679-680, 1978.

Chow, T. J., and E. D. Goldberg, On the marine geochemistry of barium, *Geochim. Cosmochim. Acta*, *20*, 192 - 198, 1960.

Church, T. M., Marine barite, Ph.D. thesis, 100 pp., Univ. of Calif., San Diego, 1970.

Church, T. M., Marine barite, in *Reviews in Mineralogy*, vol. 6, edited by R.G. Burns, pp. 175-209, Mineralogical Society of America, Washington, D.C., 1976.

Church, T. M., and K. Wolgemuth, Marine barite saturation, *Earth Planet. Sci. Lett.*, *15*, 35-44, 1972.

Dehairs, F., Discrete suspended particles of barite and the barium cycle in the open ocean, Doctoral thesis, 285 pp., Vrije Univ.Brussel, Brussels, 1979.

Dehairs F., and L. Goeyens, The biogeochemistry of barium in the southern ocean, in *Belgian Scientific Research Programme on Antarctica: Scientific Results of Phase One (Oct. '85-Jan. '89)*, vol. II, part A, *Marine Geochemistry*, edited by S. Caschetto, pp. 1-100, Prime Minister's Services, Science Policy Office, Brussels, 1989.

Dehairs, F., R. Chesselet, and J. Jedwab, Discrete suspended particles of barite and the barium cycle in the

open ocean, *Earth Planet. Sci. Lett., 49*, 528-550, 1980.

Dezan, Y., Bacterial biomass and activity in North Sea and Antarctic waters, M. Sc. thesis, 111 pp., Vrije Univ. Brussel, Brussels, 1987.

Dymond, J., Particulate barium fluxes in the oceans: An indicator of new productivity (abstract), *Eos. Trans. AGU, 56*, 1275, 1986.

Eppley, R. W., and B. J. Peterson, Particulate organic matter flux and planktonic new production in the deep ocean, *Nature, 282*, 677-680, 1979.

Finlay, B. J., N. B. Hetherington, and W. Davison, Active biological participation in lacustrine barium chemistry, *Geochim. Cosmochim. Acta, 47*, 1325-1329, 1983.

Gayral, P., and J. Fresnel, *Exanthemachrysis gayraliae Lepailleur* (Prymnesiophyceae, Pavlovales): Ultrastructure et discussion taxinomique, *Protistologica, 1*, 271-282, 1979.

Goeyens, L., and F. Dehairs, Study of the remineralization process by N-15 isotope dilution experiments, in *Les Rapports des Campagnes à la Mer, MD53 / INDIGO3 , à bord du "Marion Dufresne", 3 janvier-27 février 1987*, Publ. 87-01, Fascicule 3, edited by A. Poisson and S. Caschetto, pp. 5-21, Les Publications de la Mission de Recherche des Terres Australes et Antarctiques Françaises, Paris, France, 1989.

Goffart, A., and J. -H. Hecq, Distribution of phytoplanktonic parameters in the Indian sector of the southern ocean during INDIGO 3 cruise, in *Antarctica, Proceedings of the Belgian National Colloquium on Antarctic Research, Brussels October 20, 1987*, pp. 47-166, Prime Minister's Services, Science Policy Office, Brussels, 1988.

Goldberg, E., and G. Arrhenius, Chemistry of pelagic sediments, *Geochim. Cosmochim. Acta*, 13, 153 - 212, 1958.

Grasshoff, K., A multiple channel system for nutrient analysis in seawater with analog and digital data record, in *Advances in Automated Analysis, Technicon International Symposium, Chicago*, pp. 133-145, 1969.

Hanor, J. S., Rates of barium accumulation in the Equatorial Pacific (abstract), *Geol. Soc. Am. Abstr. Programs, 4*, 526, 1972.

Harrison, W. G., Use of isotopes, in *Nitrogen in the Marine Environment*, edited by E.J. Carpenter and D.G. Capone, pp. 763-807, Academic, San Diego, Calif., 1983.

Hubert, G., N. Rieder, G. Schmitt, and W. Send, Accumulation of barium in Müller's bodies of the Loxodidae (Ciliata, Holotricha), *Z.Naturforsch., C. 30*, 422-423, 1975.

Joiris, C., W. Overloop, M. Frankignoulle, and J. M. Bouquegneau, Preliminary discusion of the results obtained in Antarctica during the austral summer 1986-1987: Plankton ecology and ecotoxicology, in *Antarctica, Proceedings of the Belgian National Colloquium on Antarctic Research, Brussels October 20, 1987*, pp. 97-113, Prime Minister's Services, Science Policy Office, Brussels, 1988.

Lancelot, C., G. Billen, and S. Mathot, Ecophysiology of phyto- and bacterioplankton growth in the southern ocean, in *Antarctica, Belgian Scientific Research Programme on Antarctica: Scientific Results of Phase One (Oct. '85 - Jan. '89)*, vol. I, *Plankton Ecology*, edited by S. Caschetto, pp. 4-97, Prime Minister's Services, Science Policy Office, Brussels, 1989.

Le Jehan, S., and P. Tréguer, The distribution of inorganic nitrogen, phosphorus, silicon and dissolved organic matter in surface and deep waters of the southern ocean, in *Antarctic Nutrient Cycles and Food Webs* , edited by W.R. Siegfrid et al., pp. 22-29, Springer-Verlag, New York, 1983.

Lutjeharms, J. R. E., N. H. Walters, and B. R. Allanson, Oceanic frontal systems and biological enhancement, in *Antarctic Nutrient Cycles and Food Webs*, edited by W.R. Siegfrid et al., pp. 11-21 , Springer-Verlag, New York, 1983.

Mantisi, F., Utilisation des fréons 11 et 12 comme traceurs des masses d'eaux océaniques dans l'océan Indien sud ouest, Perspectives quant à la pénétration du CO_2 anthropique, Thèse de Doctorat, 178 pp., Univ.Paris 6, Paris, 1989.

Peng, T. -H., and W. S. Broecker, C / P ratios in marine detritus, *Global Biogeochem. Cycles, 1*, 155-161, 1987.

Poisson, A., B. Schauer, and C. Brunet, *Les Rapports des campagnes à la Mer, MD 53 / INDIGO 3 à bord du "Marion Dufresne", 3 janvier -27 février 1987*, Publ. 87-01, Fascicule 2, 269 pp., Les Publications de la Mission de Recherche des Terres Australes et Antarctiques Françaises, Paris, 1990.

Raeymakers, B., Characterization of particles by automated electron probe microanalysis, Doctoral thesis, 295 pp., Univ. of Antwerp, Antwerp, Belgium 1986.

Redfield, A. C., B. H. Ketchum, and F. A. Richards, The influence of organisms on the composition of seawater, in *The Sea* , vol. 2, edited by M.N. Hill, pp. 26-77, Interscience, New York, 1963.

Rhein M., and R. Schlitzer, Radium-226 and barium sources in the deep east Atlantic, *Deep Sea Res., 35*, 1499-1510, 1989.

Schmitz, B., Barium, equatorial high productivity, and the northward wandering of the Indian continent, *Paleoceanography, 2*, 63-77, 1987.

Storms, H., Quantification of automated electron microprobe X-ray analysis and application in aerosol research, Doctoral thesis, 270 pp., Univ. of Antwerp, Antwerp, Belgium, 1988.

Takahashi, T., W. S. Broecker, and S. Langer, Redfield ratio based on chemical data from isopycnal surfaces, *J. Geophys. Res., 90*, 6907-6924, 1985.

Toggweiler, J. R., K. Dixon, and K. Bryan, Simulations of radiocarbon in a coarse-resolution world model, 1, Steady state prebomb distributions, *J. Geophys. Res., 94*, 8217-8242, 1989.

Wefer, G., E. Suess, W. Balzer, G. Liebezeit, P. J. Müller, C. A. Ungerer, and W. Zenk, Fluxes of biogenic components from sediment trap deployment in circumpolar waters of the Drake Passage, *Nature, 299*, 145-147, 1982.

Whithworth, T., III, and W. D. Nowlin, Jr., Water masses and currents of the southern ocean at the Greenwich meridian, *J. Geophys. Res., 92*, 6462-6476, 1987.

P. Bernard, Departement Scheikunde, Universitaire Instelling Antwerpen, Universiteitsplein 1, B-2610 Wilrijk, Belgium.
R. Chesselet, CNRS-INSU, 15, Quai Anatole France, 75700 Paris, France.
F. Dehairs, L. Goeyens, and N. Stroobants, ANCH, Vrije Universiteit Brussel, Pleinlaan 2, B-1050 Brussels, Belgium.
C. Goyet and A. Poisson, LPCM, Université Pierre et Marie Curie, Tour 24-25, 4 Place Jussieu, 75230 Paris, France.

(Received February 15, 1990;
revised June 14, 1990;
accepted July 17, 1990.)